

Light-sheet functional imaging in fictively behaving zebrafish

To the Editor: The processing of sensory input and the generation of behavior involves large networks of neurons^{1,2}, which necessitates new technology^{3–7} for recording from many neurons in behaving animals. In the larval zebrafish, light-sheet microscopy can be used to record the activity of almost all neurons in the brain simultaneously at single-cell resolution^{3,4}. Existing implementations, however, cannot be combined with visually driven behavior because the light sheet scans over the eye, interfering with presentation of controlled visual stimuli. Here we describe a system that overcomes the confounding eye stimulation through the use of two light sheets and combines whole-brain light-sheet imaging³ with virtual reality for fictively behaving¹ larval zebrafish.

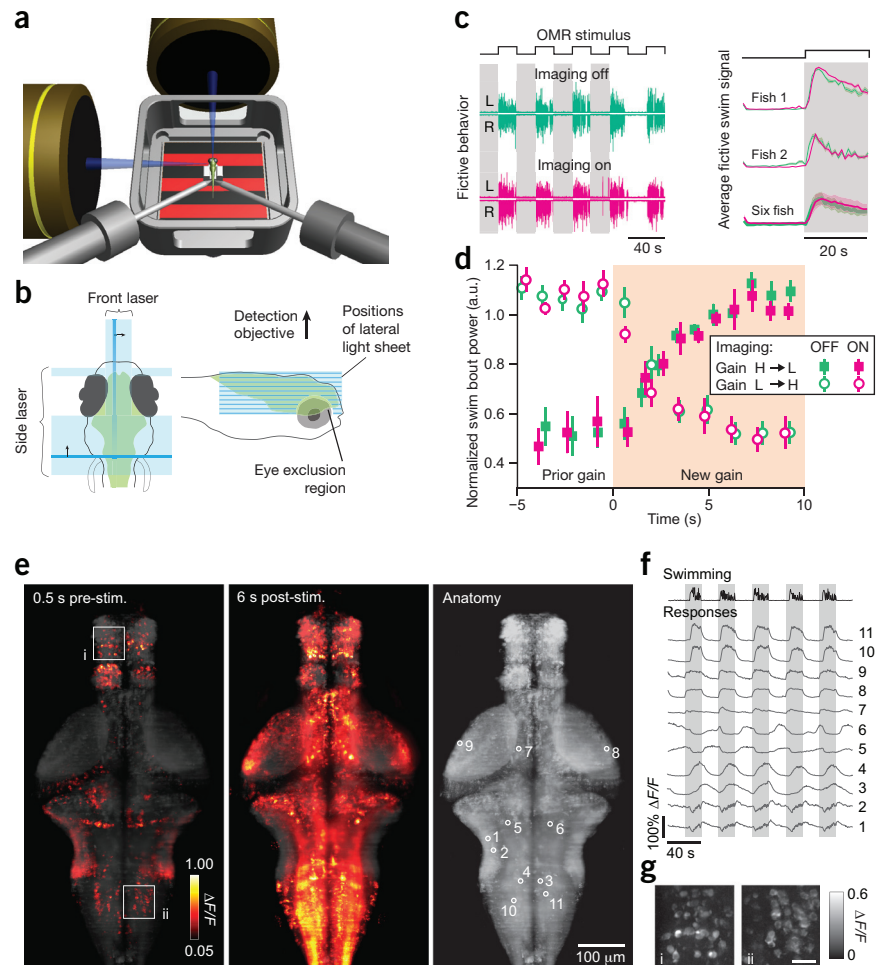
We developed a light-sheet microscopy system that scans the entire brain while avoiding direct exposure of the zebrafish retina to the excitation laser (Fig. 1a,b, Supplementary Fig. 1 and Supplementary Table 1). The system con-

sists of two excitation laser beams. One beam scans the volume of the brain from the side of a horizontally positioned zebrafish but is rapidly switched off when inside an elliptical exclusion region located over the eye (Fig. 1b). Simultaneously, a second beam scans from the front, to cover the forebrain and the regions between the eyes. Together, these two beams achieve nearly complete coverage of the brain without exposing the retina to direct laser excitation, which allows unimpeded presentation of visual stimuli that are projected onto a screen below the fish. To monitor intended swimming behavior, we used existing methods for recording activity from motor neuron axons in the tail of paralyzed larval zebrafish¹ (Fig. 1a and Supplementary Note). This system provides imaging speeds of up to three brain volumes per second (40 planes per brain volume); increases in camera speed will allow for faster volumetric sampling.

Because light-sheet imaging may still introduce some additional sensory stimulation (excitation light scattering in the brain and reflected from the glass walls of the chamber), we assessed whether fictive behavior in 5–7 d post-fertilization (d.p.f.) fish was robust to the presence of the light sheets. We tested two visuo-

Figure 1 | Whole-brain functional light-sheet imaging of fictively behaving zebrafish.

(a) Illustration of experimental setup in which two laser beams enter through windows in a custom chamber and scan the brain of a paralyzed larval zebrafish positioned above a diffusive screen on which visual scenes are projected. Two extracellular suction electrodes record fictive swimming from the tail. The detection objective located above the chamber is not shown. (b) Schematic of the laser-scanning strategy. (c) Swim signals (L, left signal; R, right signal) during the OMR (left), which was evoked by forward-moving gratings (white bars). Swim power (right) averaged across trials within individual fish (top) and averaged across fish (bottom). Error bars (shaded regions), s.e.m., $n = 6$. (d) Gain adaptation behavior during light-sheet imaging. Each data point represents the normalized power of individual swim bouts before or after gain change. Error bars, s.e.m., $n = 8$. (e–g) Whole-brain functional imaging during behavior in a fish with pan-neuronal, stable expression of cytoplasmic GCaMP6s⁸ under the *elavl3* promoter. Maximum-intensity projection of $\Delta F/F$ over the entire volume, for two time points (e), shown using a color code (0.5 s before onset of grating movement and 6 s after it; averaged over 24 trials). Anatomy is indicated using the maximum-intensity projection of mean fluorescence (gray). (f) Activity of single neurons or patches of neuropil selected by hand, during fictive behavior. (g) Magnification of regions boxed in e, showing single-neuron resolution. Scale bar, 20 μm .



motor behaviors. The first was the forward optomotor response (OMR)^{1,2}, in which swimming is elicited by visual gratings moving in the tail-to-head direction. In our system, the OMR during light-sheet scanning was comparable to the OMR without the presence of the light sheets (Fig. 1c). We defined an optomotor index as the difference in swimming strength during and before stimulus presentation. This index was significantly positive in all fish tested, with or without the laser ($P = 0.031$ with laser and $P = 0.031$ without it; two-sided sign test, $n = 6$ fish), and its magnitude was comparable between the two conditions (optomotor index: 0.67 ± 0.13 with the laser and 0.72 ± 0.067 without it, mean \pm s.d.; $P = 0.22$, two-sided paired sign test).

We also tested a more complex behavior: fictive motor adaptation, where the fish adapts its motor output to the strength of visual feedback in a closed-loop paradigm¹. Again, the behavior was comparable with and without the light sheets (Fig. 1d). We defined a gain adaptation index as the ratio of swimming during low gain and high gain. This index was significantly greater than 1 in all fish tested ($P = 0.0078$ with laser and $P = 0.0078$ without it; two-sided sign test, $n = 8$). Its magnitude was also comparable between the two conditions (gain adaptation index: 2.08 ± 0.57 with the laser and 1.91 ± 0.47 without it, mean \pm s.d.; $P = 0.29$, two-sided paired sign test).

The preservation of the OMR and gain adaptation indicates that whole-brain light-sheet imaging is compatible with fictive virtual-reality assays and can be used to interrogate whole-brain activity during visuomotor behavior. As an example, we measured whole-brain activity during the OMR in a 6 d.p.f. transgenic zebrafish expressing the genetically encoded calcium indicator GCaMP6s⁸ under the pan-neuronal *elavl3* promoter (Supplementary Note). Light-sheet imaging captures stimulus and motor-dependent patterns of whole-brain neural activity (Fig. 1e and Supplementary Video 1) with single-cell resolution across most of the brain (Fig. 1f,g and Supplementary Note). Cells and neuropil distributed across the brain showed activity during the optomotor response. We additionally assessed resolution using a fish with nuclear-localized (histone H2B fusion) expression of GCaMP6s (Supplementary Note, Supplementary Figs. 2 and 3, and Supplementary Video 2). Fish lines and DNA constructs for *elavl3:GCaMP6s* and *elavl3:H2B-GCaMP6s* are available upon request.

We presented a system for monitoring neural activity, at the cellular level, across the entire brain of the larval zebrafish during visuomotor behavior. Resources associated with this work, including sample data and analysis resources, are available via <http://research.janelia.org/zebrafish/>. This system, in combination with large-scale data analysis methods described in a companion paper⁹, holds promise for advancing the understanding of how activity in large networks of neurons underlies behavior.

Note: Any Supplementary Information and Source Data files are available in the online version of the paper (doi:10.1038/nmeth.3040).

ACKNOWLEDGMENTS

We thank M. Coleman for writing the light-sheet microscope control software Zebrascope and for continuing support; B. Coop and T. Tabachnik for their help with hardware design; S. Narayan for help with experiments; ID&F engineers for providing help on hardware components; J. Cox, R. Larson, J. Barber, B. Brandenburg and other vivarium staff for fish husbandry; G. Ceric, V. Samalam, K. Carlisle and R. Lines for assistance with the high-performance computer cluster; D.G.C. Hildebrand and M. Koyama for discussions; and V. Jayaraman, M. Reiser and G. Murphy for comments on the manuscript. This work was supported by the Howard Hughes Medical Institute.

AUTHOR CONTRIBUTIONS

M.B.A., P.J.K. and N.V. conceived of the project. M.B.A., P.J.K. and N.V. designed the experimental setup with contributions from D.V.B.; N.V. and M.B.A. built it. Y.M., T.K. and N.V. performed the experiments. N.V., T.K. and M.B.A. wrote the behavior software. J.F. and N.V. performed the imaging analysis. C.-T.Y. and L.L.L. developed the transgenic zebrafish. M.B.A., J.F. and N.V. wrote the paper with contributions from all authors.

COMPETING FINANCIAL INTERESTS

The authors declare no competing financial interests.

Nikita Vladimirov, Yu Mu, Takashi Kawashima, Davis V Bennett, Chao-Tsung Yang, Loren L Looger, Philipp J Keller, Jeremy Freeman & Misha B Ahrens

Janelia Farm Research Campus, Howard Hughes Medical Institute, Ashburn, Virginia, USA.

e-mail: ahrensm@janelia.hhmi.org

PUBLISHED ONLINE 27 JULY 2014; DOI:10.1038/NMETH.3040

- Ahrens, M.B. *et al. Nature* **485**, 471–477 (2012).
- Portugues, R., Feierstein, C.E., Engert, F. & Orger, M.B. *Neuron* **81**, 1328–1343 (2014).
- Ahrens, M.B., Orger, M.B., Robson, D.N., Li, J.M. & Keller, P.J. *Nat. Methods* **10**, 413–420 (2013).
- Panier, T. *et al. Front. Neural Circuits* **7**, 65 (2013).
- Broxton, M. *et al. Opt. Express* **21**, 25418–25439 (2013).
- Quirin, S., Jackson, J., Peterka, D.S. & Yuste, R. *Front. Neural Circuits* **8**, 29 (2014).
- Prevedel, R. *et al. Nat. Methods* **11**, 727–730 (2014).
- Chen, T.-W. *et al. Nature* **499**, 295–300 (2013).
- Freeman, J. *et al. Nat. Methods* doi:10.1038/nmeth.3041 (27 July 2014).

Guided visual exploration of genomic stratifications in cancer

To the Editor: Cancer is a heterogeneous disease, and molecular profiling of tumors from large cohorts has enabled characterization of new tumor subtypes. This is a prerequisite for improving personalized treatment and ultimately achieving better patient outcomes. Potential tumor subtypes can be identified with methods such as unsupervised clustering¹ or network-based stratification², which assign patients to sets based on high-dimensional molecular profiles. Detailed characterization of identified sets and their interpretation, however, remain a time-consuming exploratory process.

To address these challenges, we combined ‘StratomeX’³, an interactive visualization tool that is freely available at <http://www.caleydo.org/>, with exploration tools to efficiently compare multiple patient stratifications, to correlate patient sets with clinical information or genomic alterations and to view the differences between molecular profiles across patient sets. Although we focus on cancer genomics here, StratomeX can also be applied in other disease cohorts.

Thousands of patient stratifications can be derived from large cancer genomics datasets. This space of patient stratifications—which we call the ‘stratome’—contains stratifications based on, for example, clustering of mRNA, microRNA or protein expression matrices; the mutation or copy number status of genes; or on clinical variables. Owing to the size of the stratome and the heterogeneity of the underlying datasets, integration of computational and visual approaches is indispensable to the analyst in identifying biologically or clinically meaningful stratifications as well as clinical parameters and pathways that together provide a comprehensive view of each patient set.

StratomeX complements the network viewers, heat maps and genome browsers typically used in cancer genomics⁴